Journal of Engineering Mathematics **24**: 125–149, 1990.

Free convection in a horizontal porous layer with a partly heated or cooled wall

J. MERKIN* and G. ZHANG

*Department of Applied Mathematical Studies, University of Leeds, Leeds LS2 9JT, United Kingdom (*author for correspondence)*

Received 19 June 1989; accepted in revised form 2 October 1989

Abstract. The natural convective flow in a fluid-saturated porous medium is considered for an infinite horizontal channel with the bottom wall being partially heated or cooled. The flow and heat transfer are analysed for a range of values of the two non-dimensional parameters which define the problem, namely the Rayleigh number Ra and aspect ratio ε. Numerical solutions are obtained for $\varepsilon = 1$ and $\varepsilon = 0.1$ for both heated and cooled cases and for a range of values of Ra. In the heated case, the nature of the flow is seen to change from unicellular for smaller values of Ra to multicellular for larger Ra, with the value of Ra at this changeover being decreased as ε is decreased. Also, for this case, a range of values of Ra is found over which both unicellular and multicellular flows are possible. For the cooled case, a boundary layer is seen to develop on the bottom wall as Ra is increased for both the values of ε taken. Finally, a solution valid for $\varepsilon \ll 1$ is obtained and is compared with the numerical solutions for $\varepsilon = 0.1$.

1. Introduction

The convective flow of fluid through horizontal porous layers heated or cooled from below is of importance in many practical applications, for example, in the study of the behaviour of geothermal systems [1]. Extensive work has been done on the cavity geometry with side walls being differently heated, for example, by Daniels et al. [2] and Poulikakos and Bejan [3]. For the horizontal geometry, Cheng et al. [4] studied the free convection in island geothermal reservoirs by applying an exponential temperature distribution on the bottom heated wall, with recharge and discharge through the ocean sides. Numerical results were obtained for Rayleigh numbers as high as 2000. Elder [5, 6] considered the convective flow in a horizontal cavity with the central part of its bottom wall being heated to maintain a fixed temperature. He observed that more than one cell exists in the half cavity when the aspect ratio (defined as the ratio of the heated length to the height of the cavity) is greater than about 3. Recently, Prasad and Kulacki [7] also reported some results for this horizontal cavity geometry with a localized heated bottom wall but with the side walls as well as the unheated part of the bottom wall being assumed to be adiabatic. Their emphasis was put on revealing the effects of the Rayleigh number and the aspect ratio of the cavity (defined as the ratio of the width to the height of the cavity) on the free-convection heat transfer. Some qualitative description was given in their paper.

Much attention has also been paid to the study of the bifurcation structure or mode exchange associated with steady free convection in such a horizontal geometry with or without boundary imperfections. It is an analogue of the classical Rayleigh–Benard problem and is usually known as Lapwood convection in the porous medium case. Riley and Winters [8] studied the influence of aspect ratio and the effect of tilt on the mode exchange processes and the unfolding of the bifurcation. The influence of boundary imperfections on this bifurcation structure has been discussed in a series of papers by Rees and Riley [9, 10] and

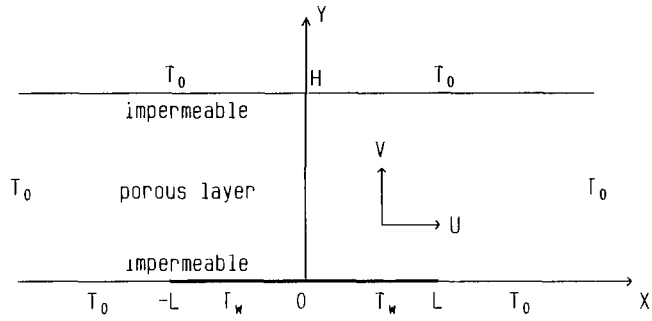

Fig. 1. The geometrical configuration.

Impey et al. [11]. The above-mentioned investigations have all been concerned with the heated case where the basic conduction region becomes unstable, and as well it is of interest to know what will happen when part of the bottom wall is maintained at a temperature lower than the ambient conditions, i.e. the bottom wall is partly cooled. Kimura et al. [12] studied the free convection near a finite cold plate facing upward in a porous medium. They found that a distinct horizontal boundary layer formed, "chopped off" to finite length by the edges of the plate. However, to our knowledge, no effort has been given to other configurations.

In this study, two-dimensional steady-state free convection in a infinite horizontal porous layer with part of its bottom wall being heated or cooled is investigated. The configuration is shown in Fig. 1 where the upper and bottom walls are assumed to be impermeable. The temperature T_w on the central part of the bottom wall is higher (heating) or lower (cooling) than the constant temperature T_0 applied on the wall away from the heated (or cooled) section. The temperature of the upper wall and porous layer at large distances from the heated section are also assumed to be T_0. The temperature of the heated section T_w is assumed to be symmetric, so that only the region $x \geqslant 0$ need be considered. The object of present study is to reveal the effects of the Rayleigh number Ra and aspect ratio $\varepsilon = H/L$ on the convection pattern and heat transfer characteristics for both the heated and cooled cases. Numerical results have been obtained for the values of Ra within a large range of interest.

For the heated case and $\varepsilon = 1$, we found that for relatively small values of Ra the flow is unicellular. Then, as Ra is increased, we found a range of values of Ra over which two different solutions exist, one with one cell, and the other with two cells. As Ra is increased further, this two-cell solution appears to be only one possible. For the cooled case, again with $\varepsilon = 1$, a boundary layer is seen to develop on the bottom wall as Ra is increased, with the flow and heat transfer becoming increasingly confined to this region. For the smaller aspect ratio of $\varepsilon = 0.1$ and the heated case, the flow quickly develops into a multicellular structure (by $\mathrm{Ra} = 7$, we found 6 cells), while for the cooled case a boundary layer again develops on the bottom wall. An analytic solution is possible when $\varepsilon \ll 1$ and Ra is of O(1), and this is used to compare with the numerical results.

2. Equations

To investigate free convection in a fluid-saturated porous layer, it is assumed that Darcy's law is valid and the fluid is assumed to be a normal Boussinesq fluid. The equations governing the conservation of mass, momentum and energy for the steady two-dimensional

flow in an isotropic, homogeneous porous medium are given by

$$\frac{\partial u}{\partial x} + \frac{\partial v}{\partial y} = 0\,, \tag{1}$$

$$u = -\frac{k}{\mu}\frac{\partial p}{\partial x}\,, \tag{2}$$

$$v = -\frac{k}{\mu}\left(\frac{\partial p}{\partial y} + \rho g\right), \tag{3}$$

$$u\frac{\partial T}{\partial x} + v\frac{\partial T}{\partial y} = \alpha\left(\frac{\partial^2 T}{\partial x^2} + \frac{\partial^2 T}{\partial y^2}\right), \tag{4}$$

$$\rho = \rho_0[1 - \beta(T - T_0)]\,, \tag{5}$$

where u and v are the velocity components as given by Darcy's law in the horizontal and vertical direction respectively; ρ, μ and β are density, viscosity and thermal expansion coefficient of the convecting fluid, k is the permeability of the porous medium, $\alpha = k/(\rho_0 c)_f$ is the effective thermal conductivity of the saturated porous medium and $(\rho_0 c)_f$ the product of density and specific heat of the convecting fluid. T, p and g are the temperature, pressure and the gravitational acceleration respectively; ρ_0 is the density when the temperature is T_0. The geometrical configuration is shown in Fig. 1.

The wall temperature $T_w(x)$ is given by

$$T_w(x) = T_0 \pm \Delta t\, \theta_w(|x|)\,, \tag{6}$$

where θ_w is a prescribed dimensionless temperature and ΔT is a measure of the applied temperature difference. The sign + is taken for the heated case and sign − for the cooled case.

To express the problem in a dimensionless form, it is natural to scale the coordinates by putting

$$\bar{x} = \frac{x}{L}\,, \qquad \bar{y} = \frac{y}{H}\,. \tag{7}$$

A suitable velocity scale is

$$U_0 = \frac{k}{u}(\rho g \beta\, \Delta T)\frac{H}{L}\,. \tag{8}$$

The velocity, pressure and temperature are then made non-dimensional by writing

$$\bar{u} = \frac{u}{U_0}\,, \qquad \bar{v} = \frac{L}{H}\frac{v}{U_0}\,, \tag{9}$$

$$\bar{p} = \frac{k}{\mu L}\frac{p}{U_0}\,, \qquad \bar{\theta} = \frac{(T - T_0)}{\Delta T}\,. \tag{10}$$

Note that the different length scales used for coordinates in (7) require, through the continuity equation (1), different scales for the velocities in (9).

Introducing the dimensionless stream function $\bar{\psi}$ defined by

$$\bar{u} = \frac{\partial \bar{\psi}}{\partial \bar{y}}, \qquad \bar{v} = -\frac{\partial \bar{\psi}}{\partial \bar{x}}, \tag{11}$$

the dimensionless form of the governing equations, after eliminating the pressure term (and on dropping bars for convenience), is

$$\varepsilon^2 \frac{\partial^2 \psi}{\partial x^2} + \frac{\partial^2 \psi}{\partial y^2} = -\frac{\partial \theta}{\partial x}, \tag{12}$$

$$\varepsilon^2 \frac{\partial^2 \theta}{\partial x^2} + \frac{\partial^2 \theta}{\partial y^2} = \varepsilon \,\mathrm{Ra}\left(\frac{\partial \psi}{\partial y}\frac{\partial \theta}{\partial x} - \frac{\partial \psi}{\partial x}\frac{\partial \theta}{\partial y}\right), \tag{13}$$

where $\varepsilon = H/L$ is the aspect ratio and Ra is the Rayleigh number defined as

$$\mathrm{Ra} = \frac{HU_0}{\alpha} = \frac{k(\rho g \beta \,\Delta T)H^2}{\alpha \mu L}. \tag{14}$$

On the impermeable walls, the boundary conditions are given by

$$\begin{aligned} &\psi = 0, \qquad \theta = \begin{cases} \pm\theta_w(|x|), & |x| \leqslant 1, \\ 0, & \text{otherwise}, \end{cases} \quad \text{on } y = 0, \\ &\psi = 0, \qquad \theta = 0 \quad \text{on } y = 1. \end{aligned} \tag{15}$$

We have taken the temperature distribution on the bottom wall such that the problem is symmetric about $x = 0$. Hence only the solution in $x \geqslant 0$ needs to be considered. The symmetry condition

$$\psi = 0, \qquad \frac{\partial \theta}{\partial x} = 0 \quad \text{on } x = 0, \qquad 0 \leqslant y \leqslant 1, \tag{16}$$

is applied on the axis of symmetry. In the region far away from the axis of symmetry, the condition of no fluid flow can assumed, and the temperature approaches the ambient one, namely

$$\psi \to 0, \qquad \theta \to 0 \quad \text{as } x \to \infty, \qquad 0 \leqslant y \leqslant 1. \tag{17}$$

The particular form of $\theta_w(x)$ is chosen to be a quadratic function in this study, namely

$$\theta_w(x) = 1 - x^2, \qquad 0 \leqslant x \leqslant 1, \tag{18}$$

though we do not expect that the qualitative form of the results will be greatly affected by different forms of $\theta_w(x)$.

3. Numerical method

We investigated the free convection flow by solving the governing equations (12) and (13) numerically. To obtain an accurate numerical solution, the boundary conditions at infinity

need to be applied at a sufficiently large distance, while for the sake of computational efficiency we require the solution domain to be of reasonable size. This suggests the use of a transformation of the x-variable and we adopted

$$\xi = \ln(1+x)/\ln 2 \tag{19}$$

which maps $x \in [0, 1]$ to $\xi \in [0, 1]$ without too much change, but for $\xi > 1$ gives a relatively large value of x for relatively small values of ξ. This feature of the transformation (19) enables us to solve the problem with a small step-length in the area above the heated or cooled section where the variation is expected to be the greatest; at the same time a reasonably small value of ξ can be used to cope with the condition at infinity. After several trial turns, we found $\xi = 3$ to be large enough for our study. The equations in terms of the transformed variable are then

$$\frac{\varepsilon^2}{2^\xi \ln 2}\frac{\partial^2\psi}{\partial\xi^2} - \frac{\varepsilon^2}{2^\xi}\frac{\partial\psi}{\partial\xi} + 2^\xi \ln 2 \frac{\partial^2\psi}{\partial y^2} = -\frac{\partial\theta}{\partial\xi}, \tag{20}$$

$$\frac{\varepsilon^2}{2^\xi \ln 2}\frac{\partial^2\theta}{\partial\xi^2} - \frac{\varepsilon^2}{2^\xi}\frac{\partial\theta}{\partial\xi} + 2^\xi \ln 2 \frac{\partial^2\theta}{\partial y^2} = \varepsilon \,\mathrm{Ra}\left(\frac{\partial\psi}{\partial y}\frac{\partial\theta}{\partial\xi} - \frac{\partial\psi}{\partial\xi}\frac{\partial\theta}{\partial y}\right). \tag{21}$$

The boundary conditions become

$$\begin{aligned}
&\psi = 0, \qquad \theta = \begin{cases} \pm 2^\xi(2-2^\xi), & 0 \leqslant \xi \leqslant 1, \\ 0, & \text{otherwise}, \end{cases} \quad \text{on } y = 0, \\
&\psi = \theta = 0 \quad \text{on } y = 1, \\
&\psi = \frac{\partial\theta}{\partial\xi} = 0 \quad \text{on } \xi = 0, \\
&\psi \to 0, \qquad \theta \to 0 \quad \text{as } \xi \to \infty.
\end{aligned} \tag{22}$$

A finite-difference grid was set up such that $\Delta\xi = \xi_\infty / M$ and $\Delta y = 1/N$, where M and N are integers (and $\xi_\infty = 3$). The first- and second-order derivatives were discretized by using central finite-differences so that the local truncation errors are $\max\{O(\Delta\xi^2), O(\Delta y^2)\}$. The discrete counterparts of equations (20) and (21) are then

$$C_1\psi_{i,j} + C_2\psi_{i+1,j} + C_3\psi_{i,j+1} + C_4\psi_{i,j-1} + C_5\psi_{i-1,j} = \gamma_1(\theta_{i+1,j} - \theta_{i-1,j}), \tag{23}$$

$$\begin{aligned}
&C_1\theta_{i,j} + C_2\theta_{i+1,j} + C_3\theta_{i,j+1} + C_4\theta_{i,j-1} + C_5\theta_{i-1,j} \\
&\quad = \gamma_2[(\psi_{i,j+1} - \psi_{i,j-1})(\theta_{i+1,j} - \theta_{i-1,j}) - (\psi_{i+1,j} - \psi_{i-1,j})(\theta_{i,j+1} - \theta_{i,j-1})]
\end{aligned} \tag{24}$$

for $i = 0, 1, \ldots, M$, $j = 1, \ldots, N$, where ψ_{ij} and $\theta_{i,j}$ are approximations of $\psi(i\,\Delta\xi, j\,\Delta y)$ and $\theta(i\,\Delta\xi, j\,\Delta y)$. The coefficients C_k, $k = 1, 2, \ldots, 5$ and γ_1, γ_2 are given by

$$C_1 = -2\left(\frac{\varepsilon^2}{\ln 2}\frac{2^{-i\,\Delta\xi}}{\Delta\xi^2} + \ln 2 \frac{2^{i\,\Delta\xi}}{\Delta y^2}\right),$$

$$C_2 = \varepsilon^2\left(\frac{1}{\ln 2}\frac{2^{-i\,\Delta\xi}}{\Delta\xi^2} - \frac{1}{2}\frac{2^{-i\,\Delta\xi}}{\Delta\xi}\right),$$

$$C_3 = C_4 = \ln 2 \frac{2^{\iota \Delta\xi}}{\Delta y^2},$$

$$C_5 = \varepsilon^2\left(\frac{1}{\ln 2}\frac{2^{-\iota \Delta\xi}}{\Delta\xi^2} + \frac{1}{2}\frac{2^{-\iota \Delta\xi}}{\Delta\xi}\right), \tag{25}$$

$$\gamma_1 = -\frac{1}{2}\frac{1}{\Delta\xi}, \qquad \gamma_2 = \frac{\varepsilon \mathrm{Ra}}{4}\frac{1}{\Delta\xi\,\Delta y}.$$

The boundary condition $\partial\theta/\partial\xi = 0$ was replaced by

$$\theta_{-1,j} = \theta_{1,j} \quad \text{for } 1 \leqslant j \leqslant N. \tag{26}$$

The treatment for the other boundary conditions is straightforward.

The coupled non-linear system of finite-difference equations (23) and (24) was solved by using an alternating Gauss–Seidel iteration; namely, starting with an initial guess for $\theta_{\iota,j}$, use equation (23) to calculate an estimate for $\psi_{\iota,j}$ by performing one step in the Gauss–Seidel iteration; these values were then used in equation (24) to calculate a new estimate for $\theta_{\iota,j}$ by the same procedure. This process was terminated if, for two successive iterations $\psi_{\iota,j}^{(k)}$, $\psi_{\iota,j}^{(k-1)}$ and $\theta_{\iota,j}^{(k)}$, $\theta_{\iota,j}^{(k-1)}$, the following criteria were satisfied simultaneously:

$$|\psi_{\iota,j}^{(k)} - \psi_{\iota,j}^{(k-1)}| < \sigma_1, \qquad |\theta_{\iota,j}^{(k)} - \theta_{\iota,j}^{(k-1)}| < \sigma_2 \tag{27}$$

where σ_1 and σ_2 were given tolerances. It was found that 10^{-6} was sufficient for both of them.

4. Results

The effects of the Rayleigh number on the free convection pattern and heat transfer characteristics were investigated both for the heated and cooled cases by fixing the aspect ratio at $\varepsilon = 1$ and increasing the values of the Rayleigh number Ra. The isotherms and streamlines are shown for selected values of Ra. The effects of the aspect ratio were then considered by obtaining the results for $\varepsilon = 0.1$. An asymptotic analysis was performed to reveal further the case where $\varepsilon \ll 1$ and Ra is of O(1). All the streamlines presented in this paper are equally spaced between the maxima and the minima of the values of the stream functions. The values of these maxima and minima are given in the captions for the figures. The isotherms (except those for the asymptotic solution) are also equally spaced between 0 and ± 1 with the bottom left one representing $\theta = \pm 0.9$ and the interval being 0.1 for the heated and cooled cases respectively.

4.1. Effects of the Rayleigh number; $\varepsilon = 1$

(a) Heated case

Figure 2 and Fig. 3 show the isotherms and streamlines, respectively, for selected values of Ra. Contours are shown only for $0 \leqslant \xi \leqslant 2$; for $\xi > 2$ the fluid was in its ambient state to the scale of the plots. For Ra = 1 the isotherms are almost the same as those for pure conduction (Ra = 0), indicating that the heat transfer is dominated by conduction when the Rayleigh

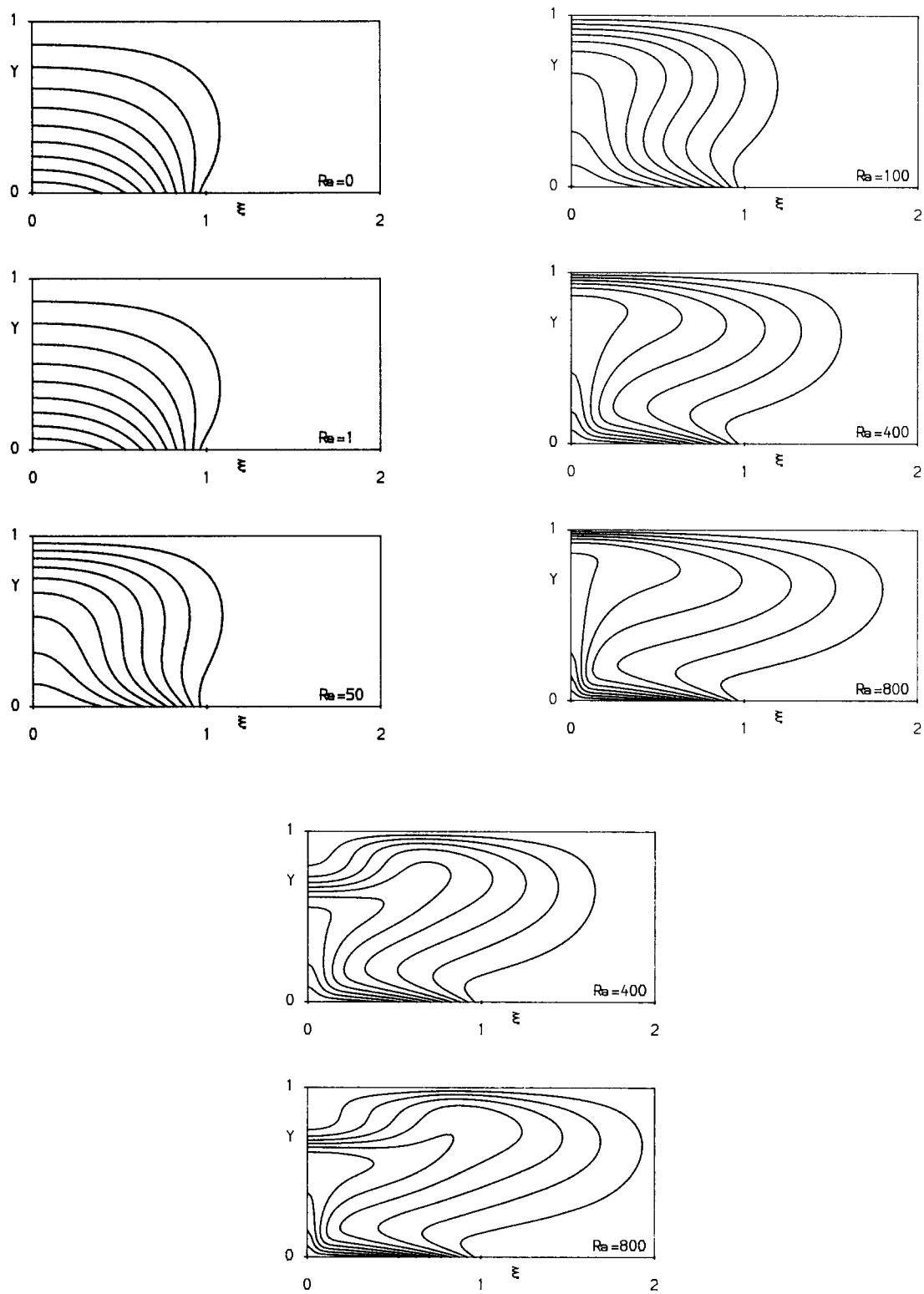

Fig. 2. Isotherms for the heated case for $\epsilon = 1$ and a range of values of Ra.

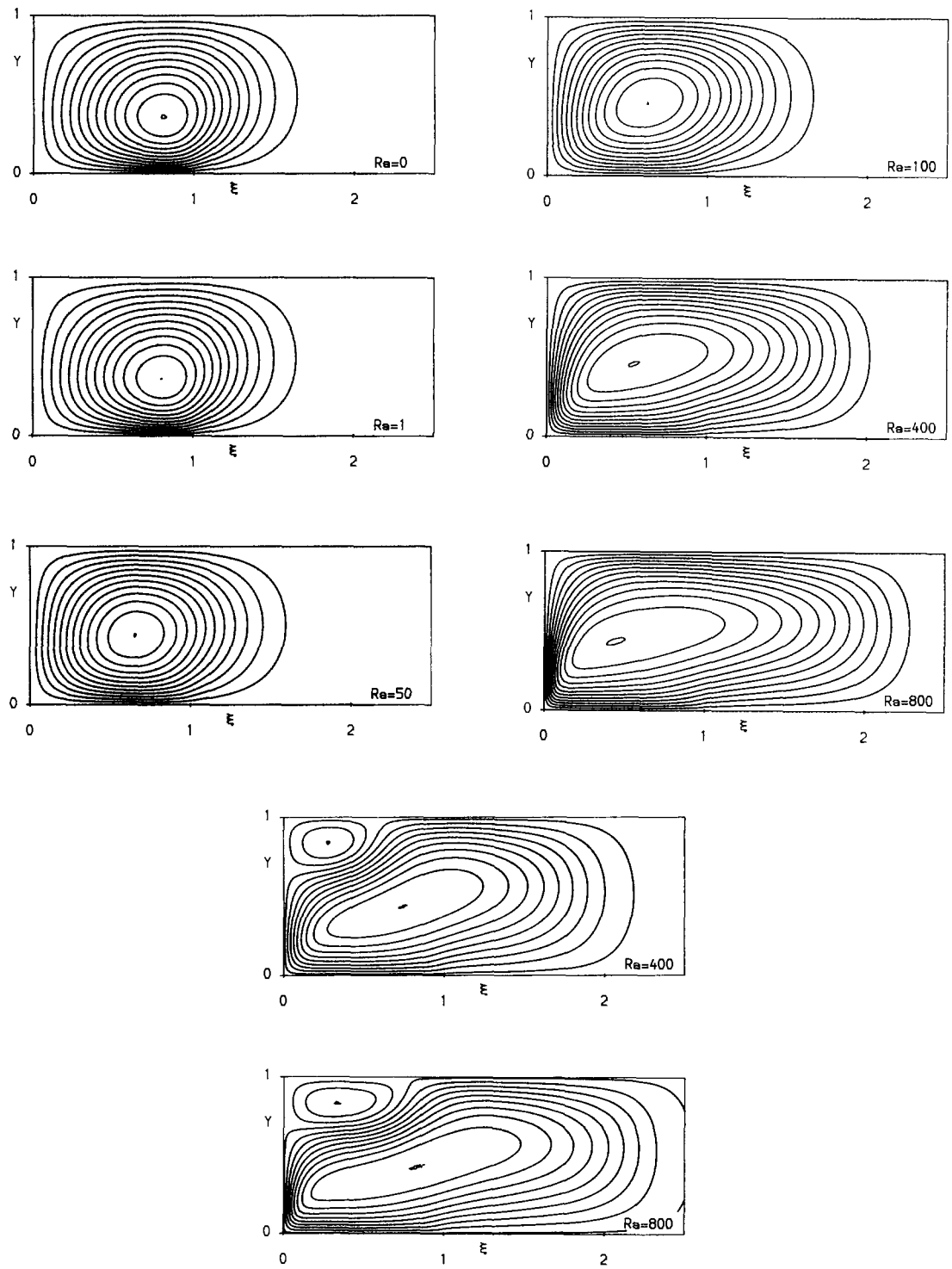

Fig. 3. Streamlines for the heated case with $\varepsilon = 1$ and a range of values of Ra. The maximum and minimum of the stream function are -0.0402, 0 at Ra = 0; -0.0406, 0 at Ra = 1; -0.0596, 0 at Ra = 50; -0.0562, 0 at Ra = 100; -0.0331, 0 at Ra = 400 (one cell); -0.0237, 0 at Ra = 800 (one cell); -0.0305, 0.0082 at Ra = 400 (two cells); -0.0214, 0.0066 at Ra = 800 (two cells).

number is low. The streamlines for Ra = 0 and Ra = 1 show that a cellular flow of clockwise circulation is set up above the heated section of the bottom wall. It is well known that there is no fluid flow for Rayleigh numbers below a certain critical value if the bottom wall is uniformly heated; Sutton [13] obtained that this critical value is $4\pi^2$ in an infinite porous layer. The reason for the occurrence of unicellular flow for Rayleigh numbers far below that critical value is due entirely to the effect of the localized heating. It is interesting to note that for these values of the Rayleigh number this cellular flow has little influence on the temperature distribution and consequently has little influence on the heat transfer.

When the Rayleigh number is increased, the isotherms are perturbed from those of the conduction-dominated regime and they develop into a half "mushroom" shape, which indicates that convection is becoming the dominant mechanism of heat transfer. The streamlines show that the fluid near the heated part of the bottom wall moves laterally towards the central region ($x = 0$) which enhances the heat transfer on the bottom wall. Near the axis of symmetry, a thermal plume is formed carrying heat to the upper portion of the central layer where the heat is transferred through the upper wall as well as being carried away by outward lateral flow along the upper wall; see Figs. 2 and 3.

When the Rayleigh number is further increased a second convection pattern emerges. This is seen to happen at a value of Ra of approximately 800. In the upper left corner, another cell emerges with counter-clockwise circulation, with the isotherms being distorted accordingly. This bicellular solution was then traced back by decreasing the values of Ra and using this bicellular solution for the initial estimates in the Gauss–Seidel iteration. It was found that there was an overlap of the values of Ra in which two possible stable solutions exist. In Figs. 2 and 3, the isotherms and streamlines for both the unicellular and bicellular solutions at Ra = 400 and 800 are shown. These figures show that there is a bifurcation from a parameter range in which just one solution exists to one where (at least) two distinct solutions are possible. Such bifurcations have been treated in some detail for viscous flow by Benjamin [14] for viscous flow and we expect that this bifurcation belongs to one of the classes of bifurcations discussed in [14]. Also, bicellular convection has been reported by El-Khatib and Prasad [15] in an investigation into the effects of stratification on thermal convection in horizontal porous cavities.

Figure 4 shows the slip velocity $U_w = (\partial\psi/\partial y)_{y=0}$ on the bottom wall for a range of values of Ra. (* represents the result corresponding to the bicellular solution at Ra = 800.) It can be

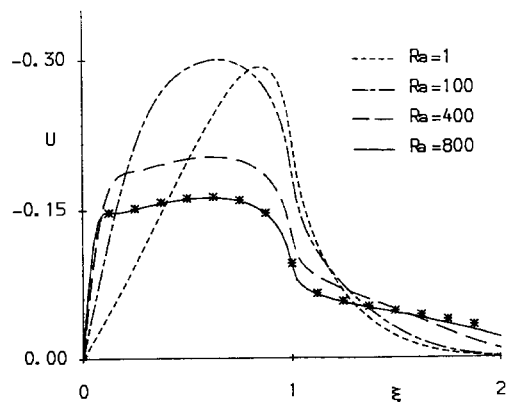

Fig. 4. Slip velocity distribution U_w on the bottom wall for the heated case with $\varepsilon = 1$. * represents the slip velocity distribution for the bicellular solution at Ra = 800.

seen that the slip velocity distribution on the heated section becomes uniform as the Rayleigh number is increased. It should be also noted that there is very little difference in the slip velocity between unicellular and bicellular solutions. This is because the secondary cell occurs in the upper left corner and has only a local influence on the overall convective flow.

In Fig. 5, we show the effect that the Rayleigh number has on the local heat-transfer rate by defining the Nusselt number as

$$\mathrm{Nu}(\xi) = -\left(\frac{\partial\theta}{\partial y}\right)_{y=0}. \tag{28}$$

It is clear that the convection enhances the heat transfer significantly for the larger values of the Rayleigh number considered (again * represents the results corresponding to the bicellular solution at Ra = 800). We can see that there is also very little difference in the heat transfer rate on the bottom wall between the one-cell and two-cell solutions.

Figure 6 shows the profiles of the horizontal velocity u across the layer at $\xi = 0.3$ and 0.6. Figure 7 shows the temperature profiles across the layer again at $\xi = 0.3$ and 0.6. (* is used in the same sense as before.) There is an initial rapid decay of the temperature near the bottom wall for Ra = 800 indicating that a thermal boundary layer is developing there. Both Figs. 6 and 7 show that the velocity and temperature profiles are only a little different for the one-cell and two-cell flows at Ra = 800.

(*b*) *Cooled case*

In Figs. 8 and 9, we present the isotherms and streamlines for a range of values of Ra when the bottom wall is partially cooled. For Ra = 0 and 1, the isotherms and streamlines are almost the same as those in the heated case apart from circulation now being counter-clockwise, which once more confirms the conclusion that the heat transfer is dominated by conduction when the Rayleigh number is low. As the Rayleigh number increases, the isotherms become confined to a region above the cooled portion of the bottom wall. The streamlines become closer together on the bottom wall near the point at which the cooling ends, i.e. at $x = 1$. The centre of the cell moves downwards towards the bottom wall with its horizontal position moving slightly beyond the line $\xi = 1$ as Ra is increased. This shows that

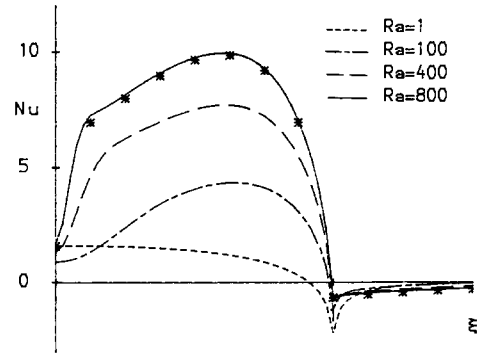

Fig. 5. Local heat transfer rate Nu on the bottom wall for the heated case with $\epsilon = 1$. * represents the results for the bicellular solution at Ra = 800.

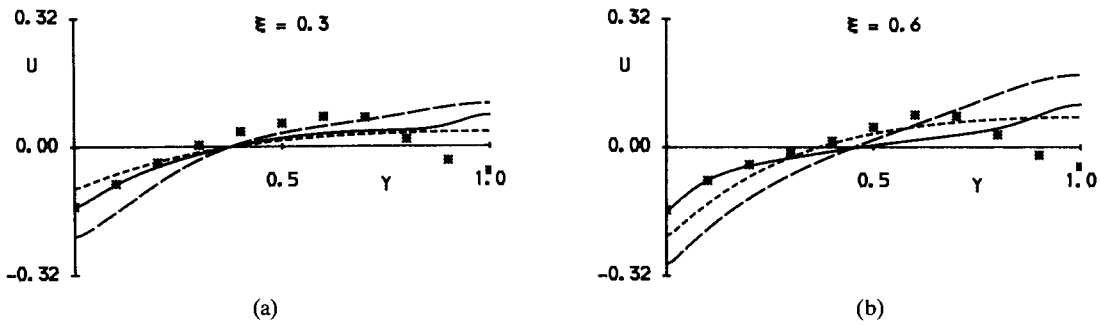

Fig. 6. Horizontal velocity distribution across the layer for the heated case with $\varepsilon = 1$. * represents the results corresponding to the bicellular solutions at Ra = 800.

a boundary layer develops with increasing Rayleigh number and by Ra = 1500 this effect is well pronounced. It is worth mentioning that the numerical solutions were somewhat easier to obtain in this case rather than in the heated case, where the iteration converged extremely slowly for values of Ra higher than 800. The slip velocity U_w and the local heat transfer rate Nu are shown in Figs. 10 and 11 respectively (where * now represents the results for Ra = 1500). From Fig. 10 we can see that the point at which the slip velocity reaches its maximum approaches the point where the cooling ends.

A boundary-layer analysis was performed to reveal further the behaviour when the value of Ra becomes large. It was found that

$$U_w \sim \mathrm{Ra}^{-1/3} \quad \text{and} \quad \mathrm{Nu} \sim \mathrm{Ra}^{1/3} \quad \text{as} \quad \mathrm{Ra} \to \infty \tag{29}$$

with the proportionality factors depending on the value of ξ. Figure 12 shows the scaled slip velocity and local heat transfer rate as suggested by (29) at $\xi = 0.5$ plotted against $\mathrm{Ra} \times 10^{-2}$. The negative value of the local heat transfer rate means that the heat flows from the layer through the bottom wall. It is clearly seen that both sets of results tend to constant values as Ra increases.

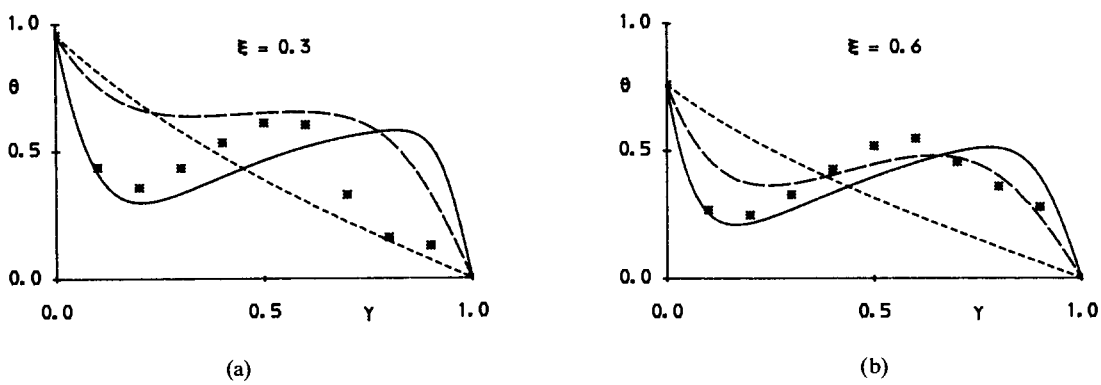

Fig. 7. Temperature distribution across the layer for the heated case with $\varepsilon = 1$. * represents the results for the bicellular solution at Ra = 800.

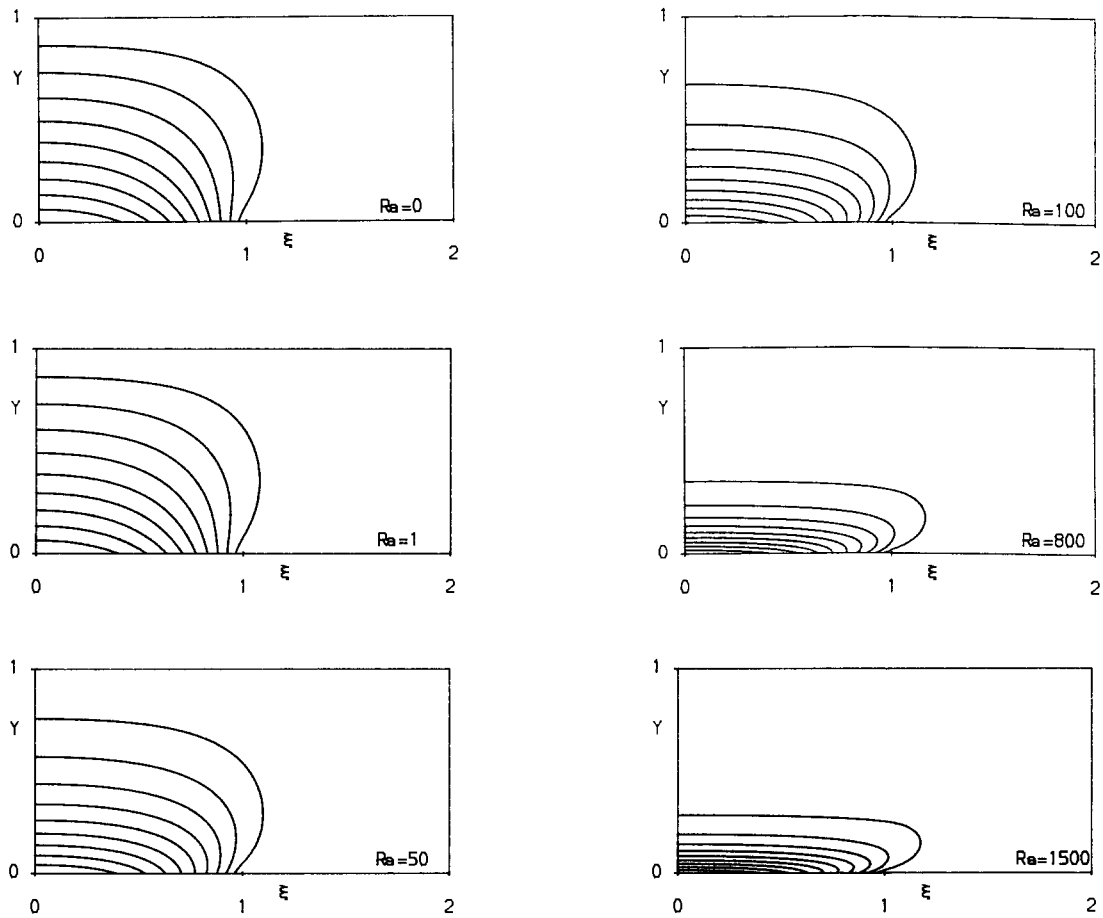

Fig. 8. Isotherms for the cooled case for $\varepsilon = 1$ and a range of values of Ra.

Figure 13 shows the profiles of the horizontal velocity u across the layer at $\xi = 0.3$ and 0.6. Figure 14 shows the temperature distribution across the layer at $\xi = 0.3$ and 0.6; (again * represents the results for Ra = 1500). The results shown in all these figures confirm that for Ra large, a boundary layer with the scalings implied by (29) develops on the bottom wall at the outer edge of which the lateral velocity and temperature both decay to zero which is the state held outside the boundary layer.

The problem of the free-convection boundary-layer flow above a cooled (or below a heated) horizontal surface has yet to be fully resolved, for either a Newtonian fluid or a porous medium. The related work of Stewartson [16] and Gill et al. [17] showed, for a Newtonian fluid, that a boundary layer starting at the edge of the plate was possible only in the heated case, with a similar result for porous media being given by Merkin and Zhang [18]. The situation for the cooled case is more complex; here the boundary layer, which must now start at the centre of the plate, is driven by the change in boundary condition at the edge of the cooled section, and any solution must take into account these two distinct effects. The existence of such boundary-layer flow has been demonstrated, for a Newtonian fluid, by Rotem [19] (experimentally) and Singh and Birkebak [20], and, for a porous medium, by our numerical solutions described above, but the analysis [20] so far has been confined to the application only of integrated forms of the boundary-layer equations.

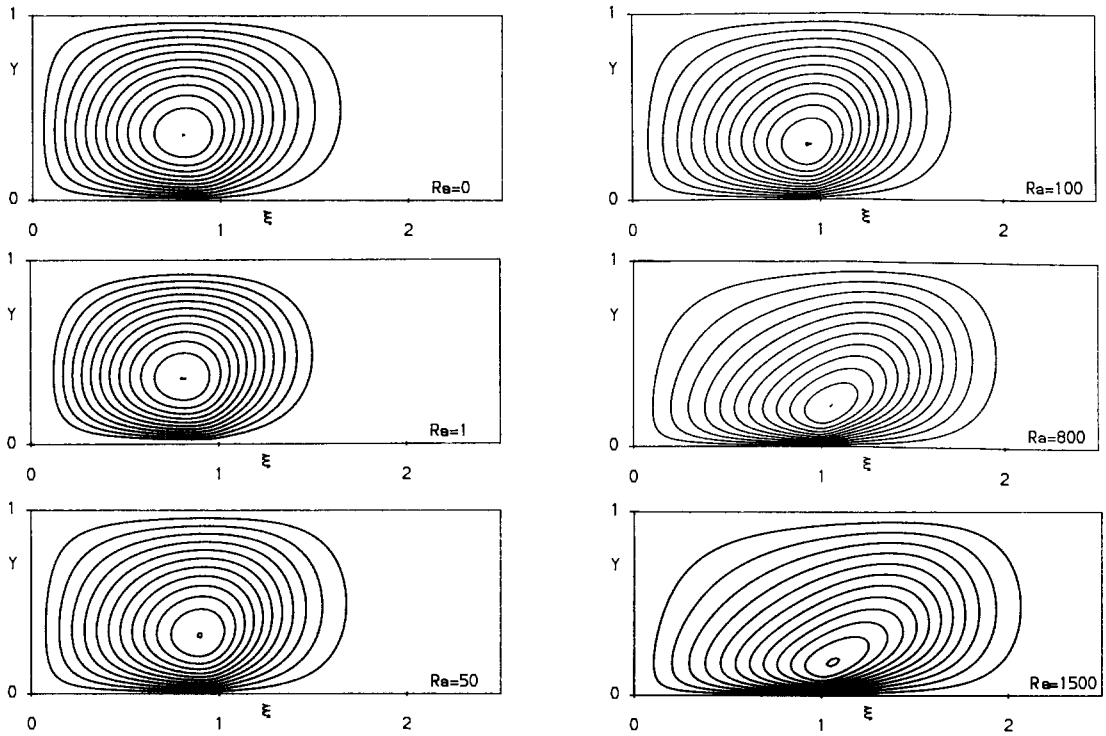

Fig. 9. Streamlines for the cooled case for $\varepsilon = 1$ and a range of values of Ra. The maxima of the stream function (the minima are zero) are 0.0399 at Ra = 0; 0.0396 at Ra = 1; 0.0289 at Ra = 50; 0.0235 at Ra = 100; 0.0087 at Ra = 800; 0.0059 at Ra = 1500.

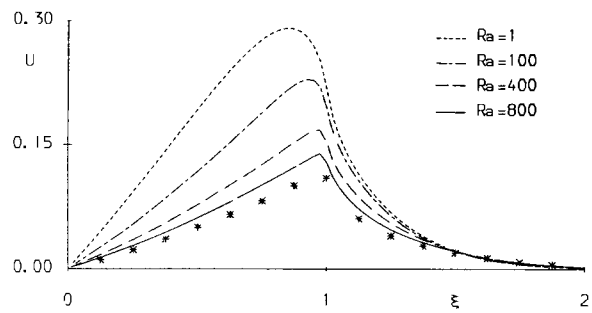

Fig. 10. Slip velocity distribution U_w on the bottom wall for the cooled case with $\varepsilon = 1$. * represents the results for Ra = 1500.

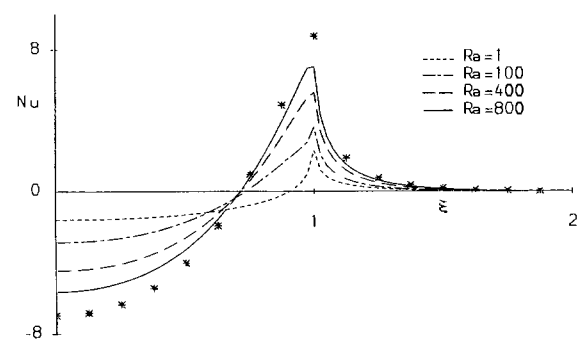

Fig. 11. Local heat transfer rate Nu on the bottom wall for the cooled case with $\varepsilon = 1$. * represents the results for Ra = 1500.

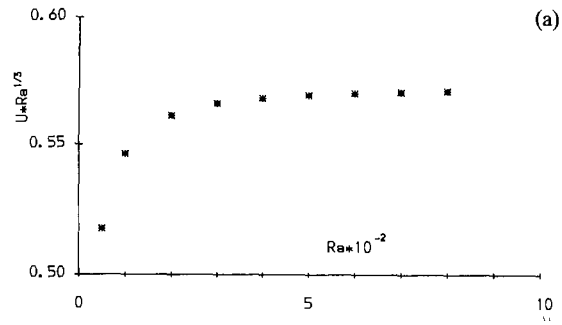

Fig. 12a. Scaled slip velocity $U_w\ \mathrm{Ra}^{1/3}$ at $\xi = 0.5$.

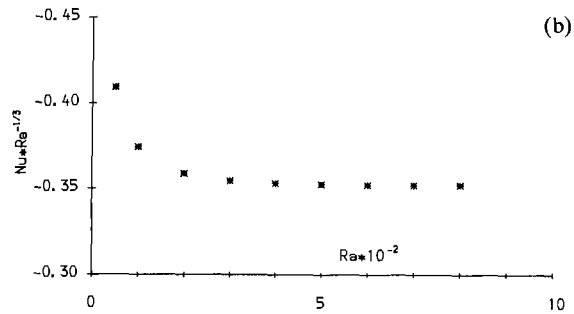

Fig. 12b. Scaled local heat transfer rate $\mathrm{Nu}\ \mathrm{Ra}^{-1/3}$ at $\xi = 0.5$.

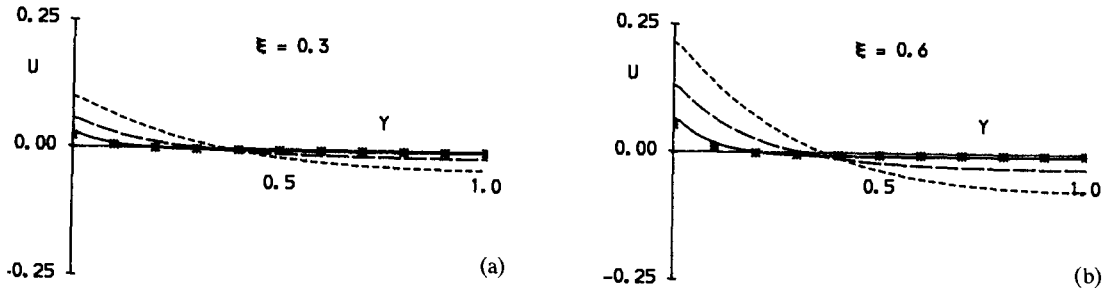

Fig. 13. Velocity distribution across the layer for cooled case with $\varepsilon = 1$.

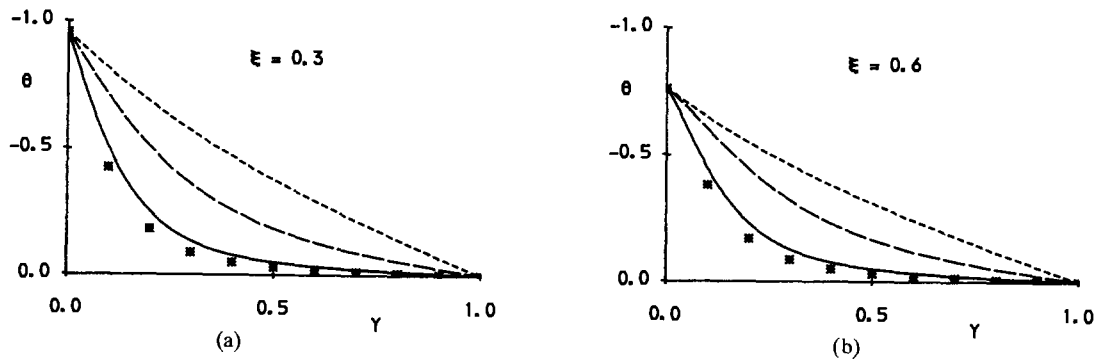

Fig. 14. Temperature distribution across the layer for the cooled case with $\varepsilon = 1$. * represents the results for Ra = 1500.

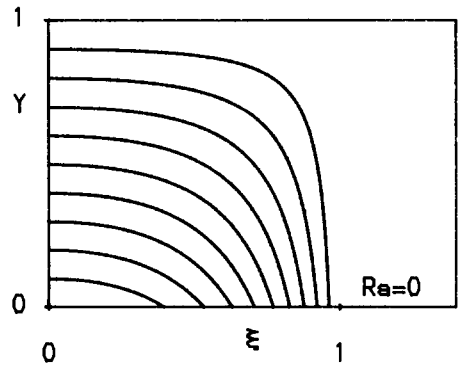

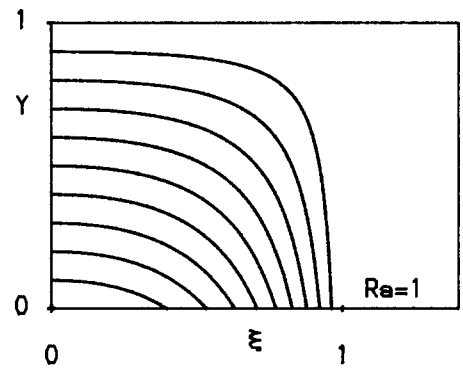

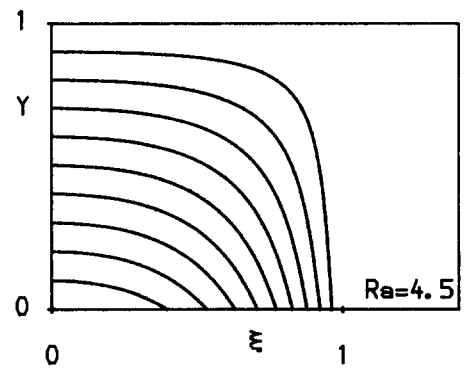

Fig. 15. Isotherms for the heated case for a range of values of Ra with $\varepsilon = 0.1$.

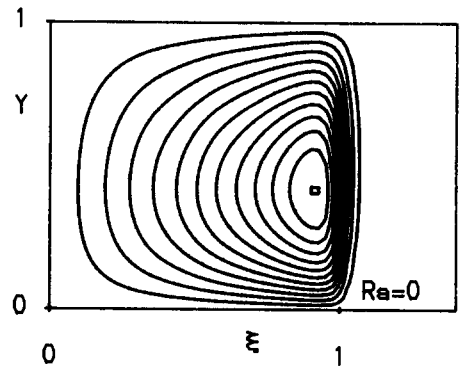

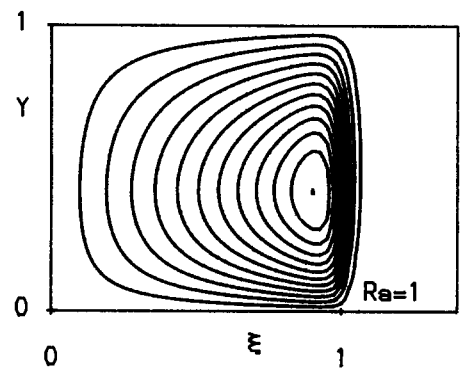

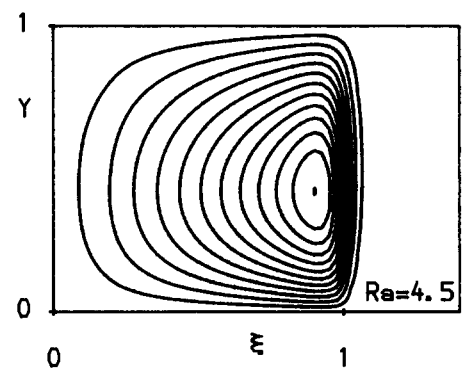

Fig. 16. Streamlines for the heated case $\varepsilon = 0.1$. The maxima and minima of the stream function are -0.1078, 0 at Ra = 0; -0.1079, 0 at Ra = 1; -0.1097, 0 at Ra = 4.5 (one cell); -0.1101, 0 at Ra = 5.4 (one cell); -0.1985, 0.1051 at Ra = 4.5 (multi-cell); -0.4272, 0.3421 at Ra = 5.4 (mutli-cell); -0.5122, 0.4698 at Ra = 7.

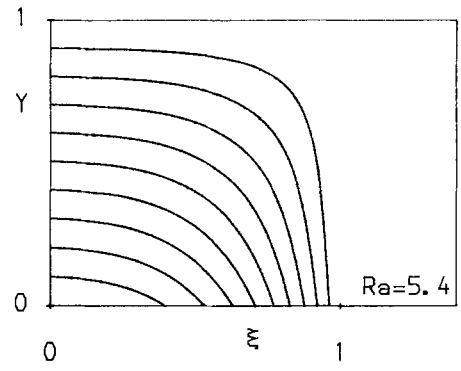

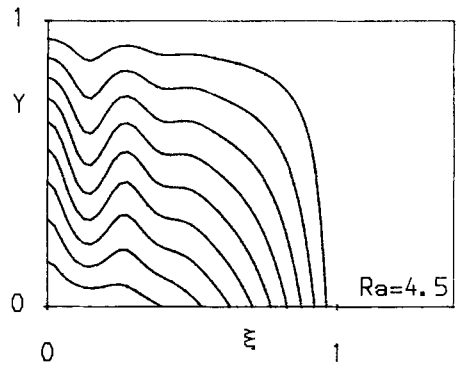

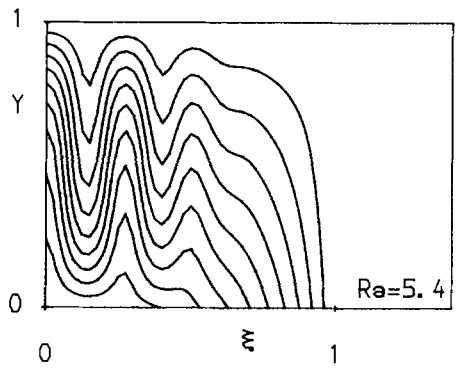

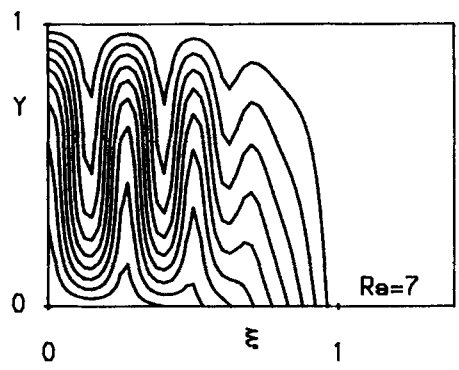

Fig. 15 (continued).

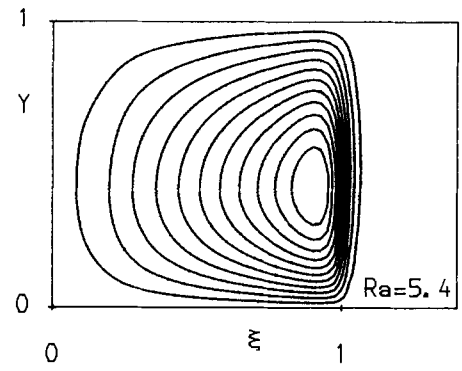

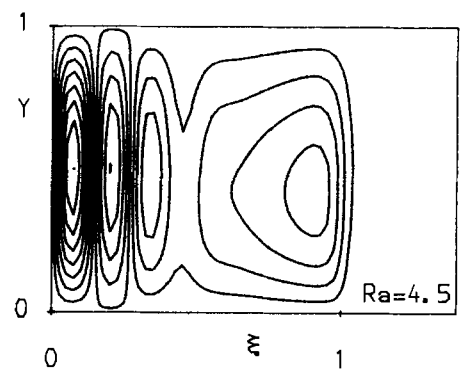

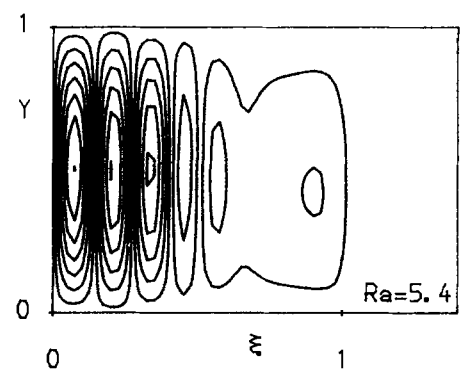

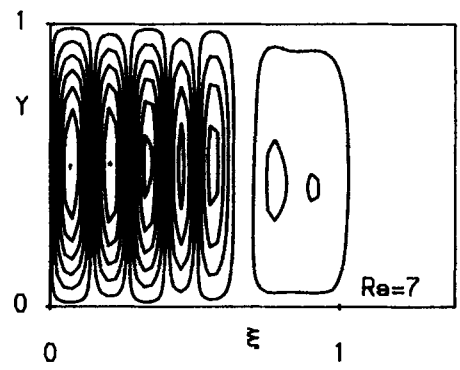

Fig. 16 (continued).

4.2. Effects of the aspect ratio

(a) Heated case

To investigate the effects of the aspect ratio on the convection pattern and heat transfer characteristics, we obtained numerical solutions for different values of ε. Figures 15 and 16 show the isotherms and streamlines respectively for $\varepsilon = 0.1$. For $\mathrm{Ra} = 1$, the isotherms are almost the same as those of pure conduction ($\mathrm{Ra} = 0$); the streamlines display a cluster close to $\xi = 1$. We also found that two stable solutions exist for some ranges of values of Ra. By increasing the value of Ra, the unicellular solution could be continued for values of the Rayleigh numbers up to about 5.4. On increasing further the value of Ra, the solution becomes multi-cellular, i.e. the streamlines form more than one cell with neighbouring cells having opposite senses of circulation. This multi-cellular solution was then continued by decreasing the value of Ra down to 4.5 at which point the solution reverted to the one-cell case. It is interesting to note that a small change of the value of Ra has little influence on the isotherms and streamlines for the unicellular solution. This is because at these low values of Ra conduction predominates for the heat transfer in this one-cell case. However, small changes in the value of Ra do have a pronounced influence on the isotherms and streamlines for the multi-cellular solutions; see Figs. 15 and 16. The number of cells depends on the value of Ra, with the cells near the axis of symmetry being more developed than the "end" cell, which breaks into more cells with the increasing of the Rayleigh number. By $\mathrm{Ra} = 7$, we can see six distinct cells. Beyond this value of Ra, it was difficult to obtain an accurate converged solution with the iteration being very sensitive to small perturbations.

As expected, this multi-cellular convection pattern greatly influences the heat transfer rate on the bottom wall. This can be seen in Figs. 17 and 18 which show the slip velocity U_w and the local heat transfer rate Nu, respectively, along the bottom wall at $\mathrm{Ra} = 1$ and at $\mathrm{Ra} = 7$.

(b) Cooled case

Figures 19 and 20 show the isotherms and streamlines for the cooled case for a range of values of Ra with $\varepsilon = 0.1$. Here no difficulty was found in obtaining fully-converged solutions up to $\mathrm{Ra} = 1500$. The flow remained unicellular throughout, and a boundary layer developed on the bottom wall as the value of Ra increased. The flow pattern and heat transfer

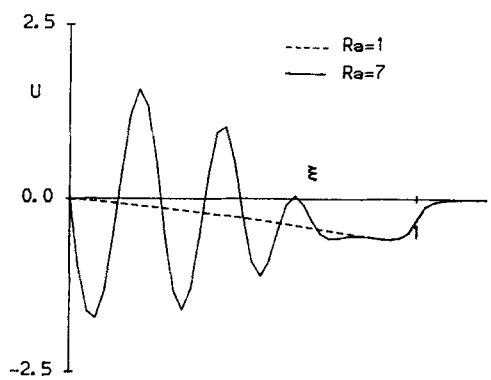

Fig. 17. Slip velocity distribution U_w on the bottom wall for the heated case for $\varepsilon = 0.1$ and $\mathrm{Ra} = 1$, $\mathrm{Ra} = 7$.

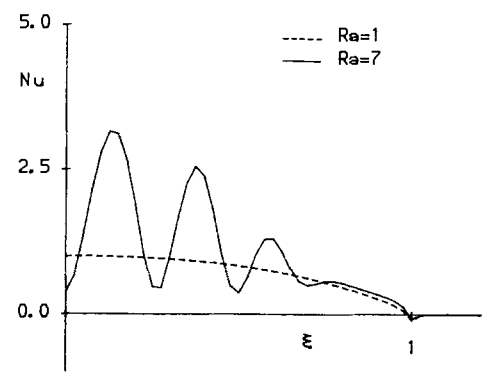

Fig. 18. Local heat transfer rate Nu on the bottom wall for the heated case for $\varepsilon = 0.1$.

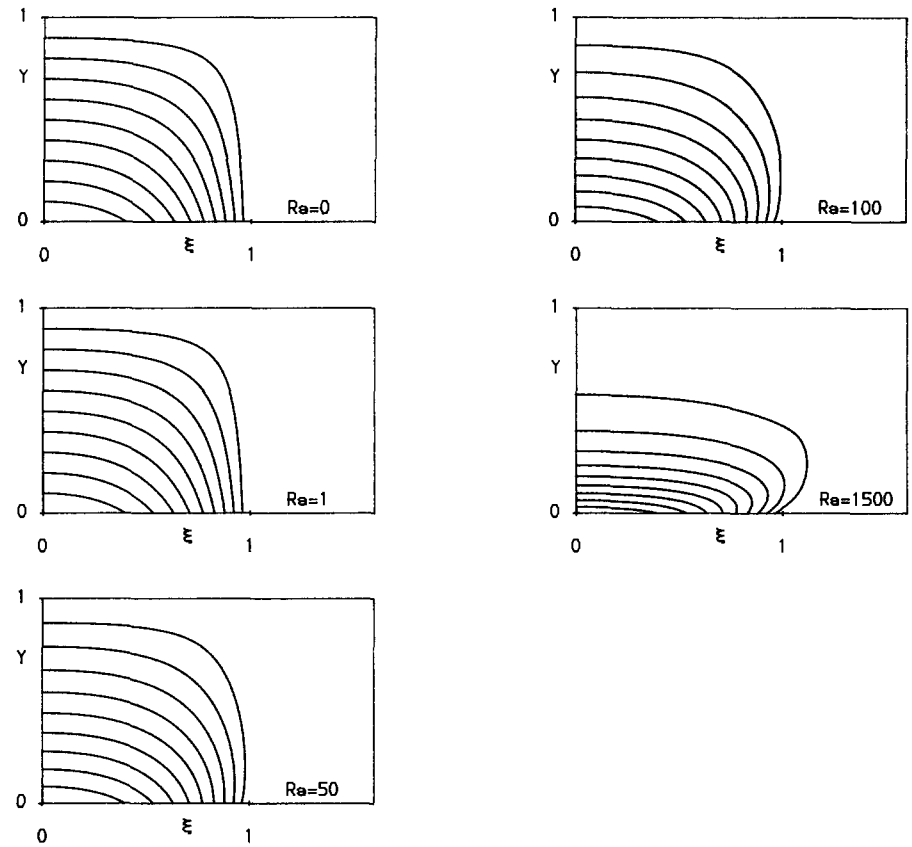

Fig. 19. Isotherms for the cooled case for a range of values of Ra with $\varepsilon = 0.1$.

characteristics were qualitatively the same as for the $\varepsilon = 1$ case, apart from the difference that for the smaller aspect ratio there is a clustering of streamlines above the point where the cooled section of the bottom wall ends. This clustering of streamlines was also observed in the unicellular flows in the heated case. This is a local effect and seems to have little overall effect on the heat transfer. So it appears that the aspect ratio is a much less important factor in determining the overall heat transfer and flow characteristics for the cooled case than it is for the heated case.

5. Narrow gap solution

Here we derive a solution of equations (12) and (13) under the assumption that

$$\varepsilon \ll 1 \quad \text{and} \quad \text{Ra is of O(1)}. \tag{30}$$

We expand the stream function ψ and the temperature θ in the form

$$\psi(x, y) = \psi_0(x, y) + \varepsilon\psi_1(x, y) + \cdots, \tag{31}$$

$$\theta(x, y) = \theta_0(x, y) + \varepsilon\theta_1(x, y) + \cdots. \tag{32}$$

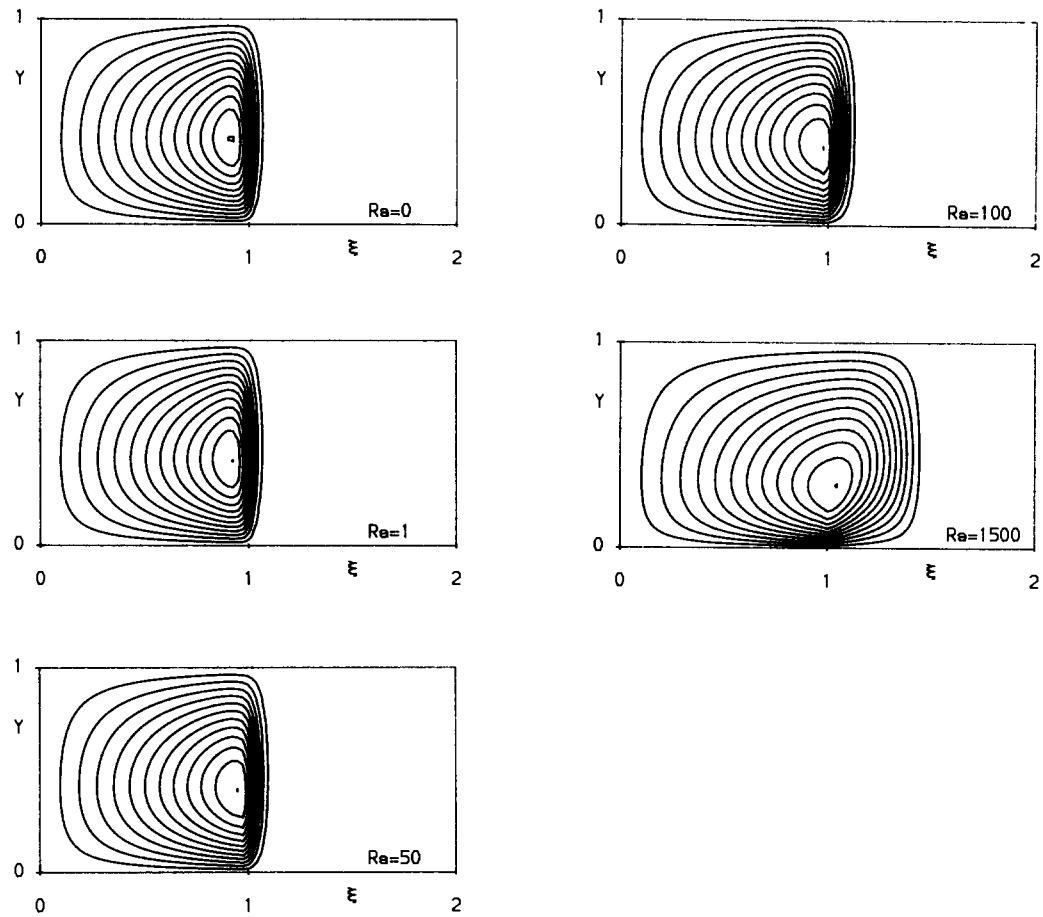

Fig. 20. Streamlines for the cooled case for a range of values of Ra with $\varepsilon = 1$. The maxima of the stream function (the minima are zero) are 0.1073 at Ra = 0; 0.1072 at Ra = 1; 0.0930 at Ra = 50; 0.0824 at Ra = 100; 0.0264 at Ra = 1500.

Substituting expansions (31) and (32) into equations (12) and (13), and solving the resulting equations gives, at leading order,

$$\theta_0(x, y) = \begin{cases} \pm\theta_w(x)(1-y), & 0 \leqslant x < 1, \\ 0, & x > 1, \end{cases} \tag{33}$$

$$\psi_0(x, y) = \begin{cases} \pm \dfrac{\theta_w'(x)}{6}\, y(1-y)(2-y), & 0 \leqslant x < 1, \\ 0, & x > 1, \end{cases} \tag{34}$$

where the upper sign is for the heated case, the lower sign for the cooled case (all double signs in the following are used in this sense) and where the prime denotes differentiation with respect to x.

The solution can be continued in a straightforward manner to $O(\varepsilon)$ and we find, in $0 \leqslant x < 1$, that

$$\theta_1(x, y) = \frac{\mathrm{Ra}\,\theta_w'^2}{360}(60y^2 - 80y^3 + 45y^4 - 9y^5 - 16y) + \frac{\mathrm{Ra}\,\theta_w\theta_w''}{360}(20y^3 - 15y^4 + 3y^5 - 8y), \tag{35}$$

$$\psi_1(x, y) = \frac{\mathrm{Ra}\,\theta_w\theta_w'''}{15120}(32y - 56y^3 + 42y^5 - 21y^6 + 3y^7) + \frac{\mathrm{Ra}\,\theta_w'\theta_w''}{15120}(64y - 280y^3 + 420y^4 - 294y^5 + 105y^6 - 15y^7) \tag{36}$$

(with $\theta_1 = 0$, $\psi_1 = 0$ in $x > 1$).

We can now examine how the solution for small ε, as given by (33) and (34), compares with the numerical solution for $\varepsilon = 0.1$. With $\theta_w(x)$ given by (18) we can see that the isotherms and streamlines patterns as calculated from (33) and (34) have the same forms for the smaller values of Ra (unicellular flow) shown in Figs. 15 and 16 (for the heated case) and in Figs. 19 and 20 (for the cooled case). A more direct comparison can be made using the wall velocity U_w and the heat transfer Nu. From (18), (33) and (34) we have, for the leading-order solution, $U_w = \mp x/3 + \cdots$ and $\mathrm{Nu} = \pm(1 - x^2) + \cdots$. This behaviour can be clearly seen in Figs. 17 and 18, respectively, for the numerical solution with $\mathrm{Ra} = 1$.

The solution given by (33)–(36), with θ_w as given by (18), has a discontinuity at $x = 1$, and a further region, centred on $x = 1$, is required to remove this discontinuity. It can be seen from (33) that θ is of $O(1 - x)$ and ψ is of $O(1)$ as $x \to 1$, which suggests that in this region we write

$$\psi(x, y) = \tilde{\psi}(\eta, y) + \cdots, \tag{37}$$

$$\theta(x, y) = \varepsilon\tilde{\theta}(\eta, y) + \cdots, \tag{38}$$

$$\eta = (x - 1)/\varepsilon. \tag{39}$$

This solution is then valid in a square region of width of $O(\varepsilon)$ above the point where the heating or cooling ends. On substituting (37) and (38) into equations (12) and (13) and letting $\varepsilon \to 0$, we find that $\tilde{\psi}$ and $\tilde{\theta}$ satisfy the equations

$$\frac{\partial^2\tilde{\psi}}{\partial\eta^2} + \frac{\partial^2\tilde{\psi}}{\partial y^2} = -\frac{\partial\tilde{\theta}}{\partial\eta}, \tag{40}$$

$$\frac{\partial^2\tilde{\theta}}{\partial\eta^2} + \frac{\partial^2\tilde{\theta}}{\partial y^2} = \mathrm{Ra}\left(\frac{\partial\tilde{\psi}}{\partial y}\frac{\partial\tilde{\theta}}{\partial\eta} - \frac{\partial\tilde{\psi}}{\partial\eta}\frac{\partial\tilde{\theta}}{\partial y}\right). \tag{41}$$

To complete the problem, the matching condition as $\eta \to -\infty$ needs to be evaluated. To do this we substitute transformation (39) into the solutions given by (33)–(36) and then let $\varepsilon \to 0$, noting that to obtain the leading-order term $\tilde{\theta}$ we need to consider both the terms θ_0 and θ_1 in expansion (32). This gives the boundary conditions

$$\tilde{\psi} \sim \mp \frac{1}{3}(2y - 3y^2 + y^3), \tag{42}$$

$$\tilde{\theta} \sim \mp 2\eta(1-y) + \frac{\mathrm{Ra}}{90}(60y^2 - 80y^3 + 45y^4 - 9y^5 - 16y). \tag{43}$$

as $\eta \to -\infty$, $0 \leqslant y \leqslant 1$; as well as

$$\begin{aligned}
&\tilde{\psi} \to 0, \quad \tilde{\theta} \to 0 \quad \text{as } \eta \to +\infty, \quad 0 \leqslant y \leqslant 1, \\
&\tilde{\psi} = 0, \quad \tilde{\theta} = 0 \quad \text{on } y = 1, \\
&\tilde{\psi} = 0, \quad \tilde{\theta} = 0 \quad \text{on } y = 0, \quad 0 \leqslant \eta < \infty, \\
&\tilde{\psi} = 0, \quad \tilde{\theta} = \mp 2\eta \quad \text{on } y = 0, \quad -\infty < \eta < 0.
\end{aligned} \tag{44}$$

The problem given by equations (40) and (41), and boundary conditions (42)–(44) has to be solved numerically and to do this we first apply the transformation

$$\eta = -\cot \zeta \tag{45}$$

which maps $(0, \pi)$ in ζ to $(-\infty, +\infty)$ in η. It should be pointed out that the matching condition as $\eta \to -\infty$, or equivalently $\zeta \to 0$, is a singular condition. A further transformation

$$\Theta = \tilde{\theta} \mp \frac{2}{\zeta}(1-y) \tag{46}$$

was introduced to cope with this singularity. Finally the equations become

$$\sin^4\zeta \frac{\partial^2\tilde{\psi}}{\partial\zeta^2} + \sin 2\zeta \sin^2\zeta \frac{\partial\tilde{\psi}}{\partial\zeta} + \frac{\partial^2\tilde{\psi}}{\partial y^2} = -\sin^2\zeta \frac{\partial\Theta}{\partial\zeta} \pm 2\frac{\sin^2\zeta}{\zeta^2}(1-y), \tag{47}$$

$$\begin{aligned}
\sin^4\zeta \frac{\partial^2\Theta}{\partial\zeta^2} + \sin 2\zeta \sin^2\zeta \frac{\partial\Theta}{\partial\zeta} + \frac{\partial^2\Theta}{\partial y^2} &= \mathrm{Ra} \sin^2\zeta \left(\frac{\partial\tilde{\psi}}{\partial y}\frac{\partial\Theta}{\partial\zeta} - \frac{\partial\tilde{\psi}}{\partial\zeta}\frac{\partial\Theta}{\partial y}\right) \\
&\mp 2\,\mathrm{Ra}\frac{\sin^2\zeta}{\zeta}(1-y)\frac{\partial\tilde{\psi}}{\partial y} \pm 2\,\mathrm{Ra}\frac{\sin^2\zeta}{\zeta}\frac{\partial\tilde{\psi}}{\partial\zeta} \\
&\mp 4\frac{\sin^4\zeta}{\zeta^3}(1-y) \pm 2\frac{\sin 2\zeta \sin^2\zeta}{\zeta^2}(1-y)
\end{aligned} \tag{48}$$

together with the boundary conditions

$$\tilde{\psi} = \mp \frac{1}{3}(2y - 3y^2 + y^3), \tag{49}$$

$$\Theta = \frac{\mathrm{Ra}}{90}(60y^2 - 80y^3 + 45y^4 - 9y^5 - 16y) \tag{50}$$

on $\zeta = 0$;

$$\tilde{\psi} = 0\,, \qquad \Theta = \mp \frac{2}{\pi}(1-y) \quad \text{on } \zeta = \pi\,, \qquad 0 < y < 1\,,$$

$$\tilde{\psi} = 0\,, \qquad \Theta = 0 \quad \text{on } y = 1\,, \qquad 0 < \zeta < \pi\,,$$

$$\tilde{\psi} = 0\,, \qquad \Theta = \mp \frac{2}{\zeta} \quad \text{on } y = 0\,, \qquad \frac{\pi}{2} \leqslant \zeta < \pi\,,$$

$$\tilde{\psi} = 0\,, \qquad \Theta = \pm 2\cot\zeta \mp \frac{2}{\zeta} \quad \text{on } y = 0\,, \qquad 0 < \zeta < \frac{\pi}{2}\,. \tag{51}$$

Equations (47) and (48) subject to boundary conditions (49)–(51) were solved by a procedure similar to that described above for the general problem. Figures 21 and 22 show isotherms and streamlines for the heated case, and Figs. 23 and 24 for the cooled case. The results displayed in these figures are in terms of $\tilde{\theta}$ and $\tilde{\psi}$ in the (ζ, y)-plane; $\zeta = \pi/2$ (≈ 1.57) corresponds to $x = 0$ in the original coordinate system. Since $\tilde{\theta}$ tends to infinity as $\zeta \to 0$, the isotherms are presented by prescribing $\tilde{\theta}$ at $\zeta = 0$ as

$$\tilde{\theta}(0, y) = \pm 2 \times 10^4 (1 - y)\,. \tag{52}$$

The isotherms are equally spaced with the interval being 0.8. The streamlines are also equally spaced with the minimum in the heated case and the maximum in the cooled case being ∓ 0.013, respectively. As for the general problem, it was found to be much easier to obtain converged solutions for this problem for the cooled case than for the heated case. In this latter case, solutions could be obtained up to about Ra = 7 at which point the streamline

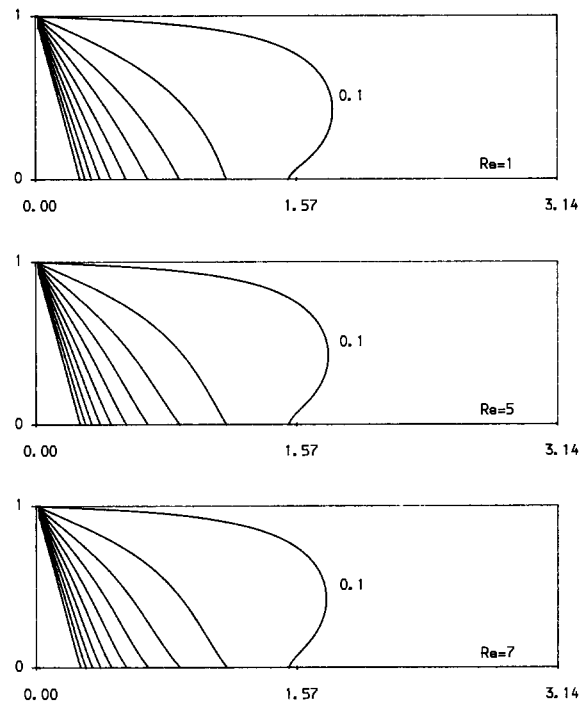

Fig. 21. Isotherms of the narrow gap solution; heated case.

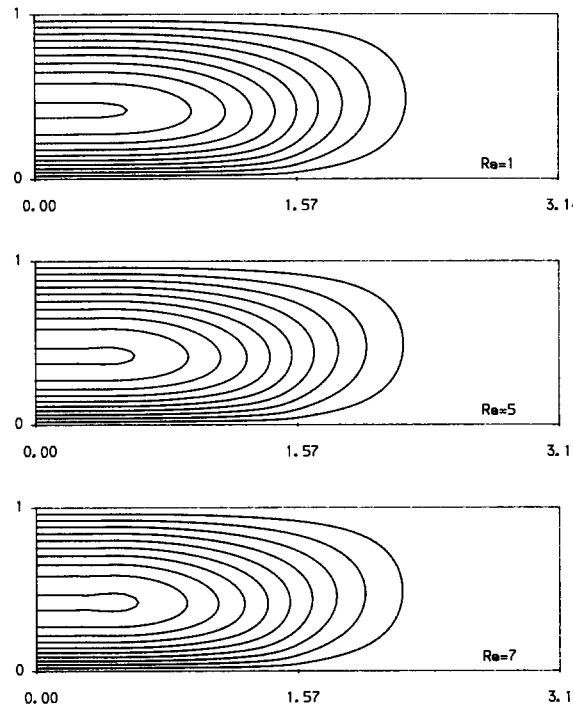

Fig. 22. Streamlines of the narrow gap solution; heated case.

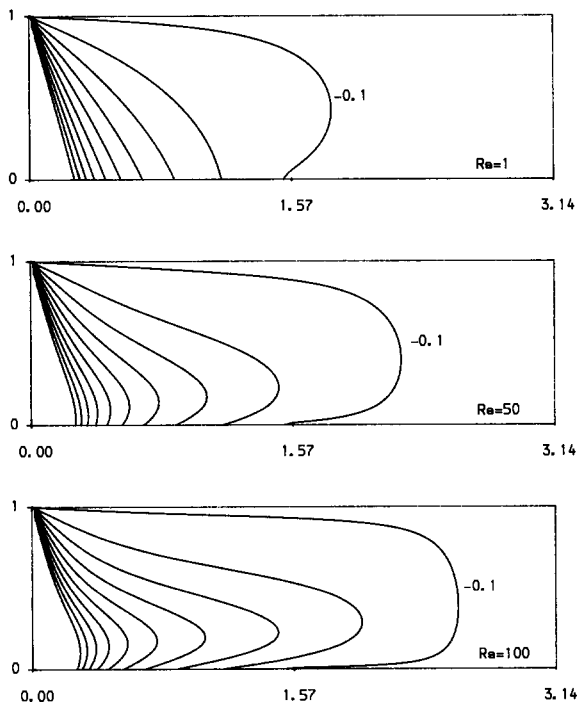

Fig. 23. Isotherms of the narrow gap solution; cooled case.

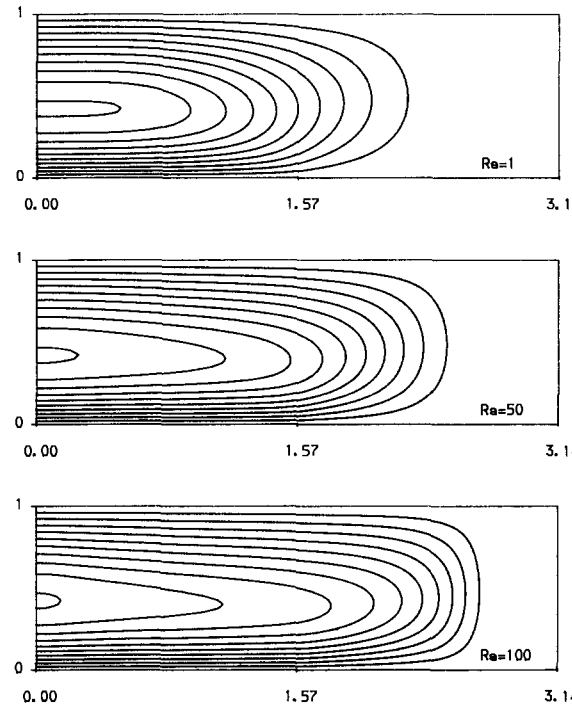

Fig. 24. Streamlines of the narrow gap solution; cooled case.

plots suggested the break-up into subsidiary eddies. This is in line with the numerical solutions for $\varepsilon = 0.1$, where we could obtain a unicellular solution for Rayleigh numbers up to about this value. No such problem was encountered for the cooled case, with it being seemingly possible to obtain solutions for any value of Ra. However, the form of the terms of $O(\varepsilon)$ in expansions (32) and (33), as given by (35) and (36), require that $\varepsilon\,\mathrm{Ra} \ll 1$ rather than just $\varepsilon \ll 1$. It is then unrealistic to continue the solution to very high values of Ra and our results are given only up to $\mathrm{Ra} = 100$.

6. Conclusions

We have considered the effects of the Rayleigh number Ra and aspect ratio ε on the convection pattern and heat transfer characteristics for an infinite horizontal porous layer with the bottom wall being partly heated or cooled. Using a numerical solution for the heated case, we have found that two possible stable solutions exist for the values of Ra within some range. When the aspect ratio $\varepsilon = 1$, the minimum value of Ra at which the bicellular solution emerges is large (approximately 400) and the range of values of Ra which allows double solutions, i.e. both unicellular and bicellular, is also large. One of the effects of decreasing the aspect ratio is to decrease this minimum value and to reduce the range of values of Ra over which two possible stable solutions exist. The other effect is that the value of the aspect ratio determines the structure of the second solution: bicellular at $\varepsilon = 1$ and multi-cellular at $\varepsilon = 0.1$ for the problem considered above. The numerical solutions for the cooled case show that the convection pattern is always unicellular. A boundary layer develops on the bottom wall when the Rayleigh number is high. In the limiting case where

the Raleigh number tends to infinity, the lateral movement of fluid disappears everywhere except within a thin boundary layer of thickness of $O(Ra^{-1/3})$ on the bottom wall. Correspondingly, the temperature outside the boundary layer tends to the uniform ambient condition.

References

1. P. Cheng, Heat transfer in geothermal systems, *Adv. Heat Transfer* 14 (1978) 1–105.
2. P.G. Daniels, P.A. Blythe and P.G. Simpkins, Thermally driven shallow cavity flows in porous media: the intermediate regime, *Proc. Roy. Soc. Lond.* A406 (1986) 263–285.
3. D. Poulikakos and A. Bejan, Natural convection in a porous layer heated and cooled along one vertical side, *Int. J. Heat & Mass Transfer* 27 (1984) 1879–1891.
4. P. Cheng, K.C. Yeng and K.H. Lau, Numerical solutions for steady free convection in island geothermal reservoirs, *Future Energy Production Systems*, Vol. 2, pp. 429–448, Hemisphere Publishing Corp., Washington, D.C. (1976).
5. J.W. Elder, Steady free convection in a porous layer heated from below, *J. Fluid Mech.* 27 (1967) 29–48.
6. J.W. Elder, Transient convection in a porous medium, *J. Fluid Mech.* 27 (1967) 609–623.
7. V. Prasad and F.A. Kulacki, Natural convection in horizontal porous layers with localized heated from below, *ASME J. Heat Transfer* 109 (1987) 795–798.
8. D.S. Riley and K.H. Winters, The onset of convection in a porous medium: a preliminary study, AERE R 12586, Harwell Laboratory, Oxfordshire (1987).
9. D.A.S. Rees and D.S. Riley, The effects of boundary imperfections on convection in a saturated porous layer: non-resonant wavelength excitation, *Proc. Roy. Soc. Lond.* A421 (1989) 303–339.
10. D.A.S. Rees and D.S. Riley, The effects of boundary imperfections on convection in a saturated porous layer: near-resonant wavelength excitation, *J. Fluid Mech.* 199 (1989) 133–154.
11. M.D. Impey, D.S. Riley and K.H. Winters, The effect of sidewall imperfections on pattern formation in Lapwood convection, TP. 1304, Harwell Laboratory, Oxfordshire (1988).
12. S. Kimura, A. Bejan and I. Pop, Natural convection near a cold plate facing upward in a porous medium, *ASME J. Heat Tansfer* 107 (1985) 819–825.
13. F. Sutton, Onset of convection in a porous channel with net through flow, *Phys. Fluids* 13 (1970) 1931–1934.
14. T.B. Benjamin, Bifurcation phenomena in steady flows of a viscous fluid, I: Theory, *Proc. Roy. Soc. Lond.* A359 (1978) 1–26.
15. G. El-Khatib and V. Prasad, Effects of stratification on thermal convection in horizontal porous layers with localized heating, *Trans. A.S.M.E., J. Heat Transfer* 109 (1987) 683–687.
16. K. Stewartson, On the free convection from a horizontal plate, *J. Applid Math. and Physics (ZAMP)* 9 (1958) 276–281.
17. W.N. Gill, D.W. Zeh and E. Del Casal, Free convection on a horizontal plate, *J. Applied Math. and Physics (ZAMP)* 16 (1965) 539–541.
18. J.H. Merkin and G. Zhang, On the similarity solutions for free convection in a saturated porous medium adjacent to impermeable horizontal surfaces, to appear in *Wärme- und Stoffübertragung*.
19. Z. Rotem, Free convection from heated, horizontal downward-facing plates, *J. Applied Math. and Physics (ZAMP)* 21 (1970) 472–475.
20. S.W. Singh and R.C. Birkebak, Laminar free convection from a horizontal infinite strip facing downwards, *J. Applied Math. and Physics (ZAMP)* 20 (1969) 454–461.